An Initiative Towards Quality Control of Photovoltaic Panels: Local Innovation Under Constraints

Francisco Pascal Elias Tambasafidy [1]
https://orcid.org/0009-0005-1975-8983
tfpelias@gmail.com

Jean Baptiste Ratongasoandrazana [1]
https://orcid.org/0009-0000-9416-4409

Rivo Herivola Manjakamanana Ravelonjato [1, 2]
https://orcid.org/0009-0006-5658-6153

Naivo Rabesiranana [2]
https://orcid.org/0000-0003-0131-9016

Joel Rajaobelison [2]
http://orcid./0009-0005-4683-9068

Abstract

Quality control of photovoltaic panels and batteries is a key requirement for the success of the energy transition. In practice, standardised testing relies on advanced equipment that is costly and difficult to access in many low-resource settings. This work presents a locally designed electronic load system that is able to trace current–voltage (I–V) curves, to estimate maximum power output up to 300 W under natural sunlight, and to measure battery discharge capacity. The proposed approach does not replace industrial certification methods, but it allows direct comparison of different products tested under identical conditions and supports performance evaluation in real operating environments. Developed following a training workshop led by experts from MINATEC in France, this initiative shows that local technical capacity for photovoltaic quality assessment can be built using affordable and innovative tools.

Keywords: quality control; photovoltaic panels; batteries; electronic load; frugal innovation

1 Department of Maintenance and Instrumentation, National Institute of Nuclear Sciences and Techniques, Madagascar.
2 Department of Physics, University of Antananarivo, Madagascar.

Nano-Horizons
Volume 5 | 2026 | #21943 | 16 pages
https://doi.org/10.25159/3005-2602/21943
ISSN 3005-2602 (Online)

1 Introduction

Solar photovoltaic (PV) technology has become a central pillar of sustainable development, especially in regions where access to electricity remains limited [1]. Madagascar illustrates this situation clearly. Although the country receives more than 2 800 hours of sunshine per year, only about 33.7% of the population has access to electricity, and this figure falls to 7–11% in rural areas [2]. As a result, off-grid solar systems have spread rapidly. However, the quality of available products varies widely, which creates a serious risk for long-term system reliability.

International standards such as IEC 61215 and IEC 61730 require PV modules to be tested under standard test conditions (STCs) (1 000 W/m^2, 25 °C, AM 1.5 spectrum) [3]. These tests rely on expensive infrastructure, including solar simulators, climate chambers and calibrated current–voltage (I–V) tracers [3], [4]. Although mobile accredited laboratories have been developed to perform on-site testing with high precision, as demonstrated by Coello et al. [5] with their PV mobile laboratory incorporating a class A$^+$ solar simulator and climate control system, their cost and complexity remain prohibitive for many low-resource settings. The high cost of such facilities creates a major gap: regions that most need quality control tools are often those with the least access to certification laboratories. This situation weakens consumer trust, increases system failures, and slows the development of local technical skills. This challenge is not unique to Madagascar and has spurred a global trend towards frugal innovation in PV characterisation. Recent research demonstrates the feasibility of automated low-cost tools based on microcontroller platforms for performance assessment and defect detection [6]. Simultaneously, AI-powered defect detection approaches are also emerging, aiming to automate and enhance the visual inspection of modules. For instance, Hassan and Dhimish [7] developed a system based on a convolutional neural network to analyse electroluminescence images and automatically detect cracks, potential-induced degradation (PID), and shaded areas with an accuracy exceeding 98%. This work exemplifies the diversity of technological innovations aimed at strengthening quality assurance across the PV industry.

To address this issue, the present study follows principles of frugal innovation. A 300 W programmable direct current (DC) electronic load was designed and developed at the Department of Maintenance and Instrumentation of the National Institute of Nuclear Sciences and Techniques (INSTN–Madagascar) [8] using locally available components. Inspired by a training workshop conducted by experts from MINATEC in France during the First International Nanomada Colloquium in 2018 [9], this microcontroller-based system enables I–V and P–V curve tracing of PV modules under natural sunlight, as well as battery capacity measurements. The system is intended for comparative testing and for identifying underperforming or degraded products.

Although it cannot replace standardised certification procedures, this approach allows local institutions to perform meaningful quality assessments. It supports informed purchasing decisions and contributes to building technical expertise, which is essential to sustainable growth of solar markets in resource-constrained environments.

2 Methods

2.1 Theoretical Framework

2.1.1 Photovoltaic Cell Characterisation

Crystalline silicon PV cells convert solar irradiance into electrical energy through the PV effect. Their electrical behaviour is typically described by the single-diode equivalent circuit model (Figure 1). In this model, the cell is represented by a photocurrent source in parallel with a *p-n* junction diode, a series resistance (R_s), and shunt resistance (R_{sh}) [1], [3], [10].

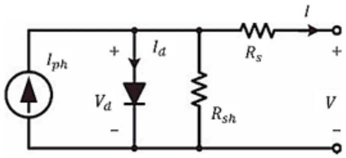

Figure 1: Single-diode equivalent circuit model of a PV cell

The current–voltage relationship is given by:

$$I = I\_ph - I\_0\,[\exp((V + IR\_s)/(nV\_t\,)) - 1] - (V + IR\_s)/R\_sh$$

where I_{ph} is the photogenerated current, proportional to incident irradiance, I_0 is the diode saturation current, n is the diode ideality factor (typically between 1 and 2 for silicon), and $V_t = kT/q$ is the thermal voltage. Here, $k = 1.381 \times 10^{-23}$ J/K is Boltzmann's constant and $q = 1.602 \times 10^{-19}$ C is the elementary charge.

The series resistance R_s represents ohmic losses due to the semiconductor material, contacts and interconnections. The shunt resistance R_{sh} accounts for leakage paths caused by manufacturing defects. A high R_s reduces the fill factor and output power, while a low R_{sh} increases leakage currents, especially at low voltages [3].

For PV modules composed of multiple cells, the overall behaviour scales accordingly. Cells connected in series increase the output voltage, while parallel connections increase the output current.

2.1.2 I–V Characteristics and Key Performance Metrics

Several key operating points define PV cell and module performance (Figure 2). The short-circuit current I_{sc} is measured at zero voltage and is approximately equal to I_{ph}. The open-circuit voltage V_{oc} is measured at zero current. The maximum power point

(MPP), defined by (V_{mpp}, I_{mpp}), corresponds to the operating point where the product $P = VI$ is maximised [3], [11].

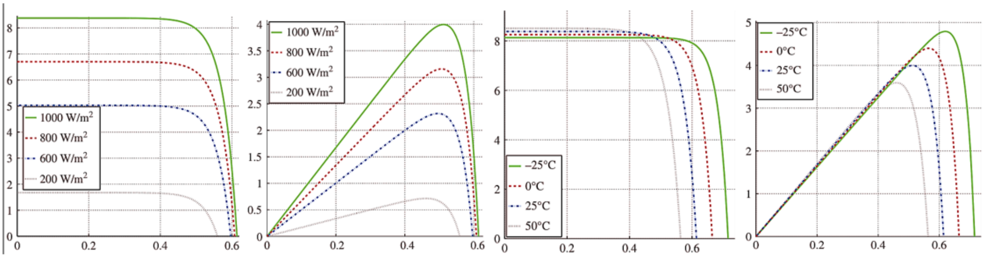

Figure 2: PV cell I–V and P–V characteristics under varying environmental conditions

The fill factor (FF) is used to quantify the quality of the $I-V$ curve. In practice, for quality assessment, key parameters such as the series resistance (R_S), shunt resistance (R_{sh}), and the FF are extracted from the measured I–V curves. These parameters serve as critical indicators of internal losses and manufacturing quality, as established in methodologies for low-cost characterisation tools [6]:

$$"FF" = (V\_mpp \times I\_mpp)/(V\_oc \times I\_sc)$$

Higher FF values indicate lower internal losses and better manufacturing quality. PV performance depends strongly on irradiance and temperature. The photocurrent increases almost linearly with irradiance, while the open-circuit voltage varies logarithmically. Increasing temperature mainly reduces V_{oc} and slightly increases I_{sc} (Figure 2) [3].

2.1.3 Battery Characterisation Fundamentals

Battery characterisation focuses on parameters such as capacity, energy, internal resistance, discharge rate effects, and state of charge (SOC) [3], [12]. The main quantities are defined as follows:

- Capacity: $Q = \int I(t)\, dt$, representing the total delivered charge in ampere-hours.
- Energy: $E = \int V(t)I(t)\, dt$, representing the total extracted energy in watt-hours.
- Peukert's law: $Q_{eff}(I) \propto I^{1-k}$, for lead-acid batteries, describing capacity reduction at higher discharge currents.
- State of charge: $\text{“SOC”}(t) = \text{“SOC”}(0) - 1/Q_{nom} \int I(\tau)\, d\tau$ estimated using coulomb counting.
- Internal resistance: $R_{int} \approx \Delta V_{inst}/\Delta I$, which increases with ageing and degradation.

2.2 System Design and Architecture

2.2.1 System Overview

The electronic load is based on a microcontroller-centred (Arduino Nano [13]) architecture with fast analogue control loops to ensure stability and precision (Figure 3). The system includes user controls, an LCD display, and the option for PC-based data logging. A closed-loop current regulation scheme allows accurate control of the load current.

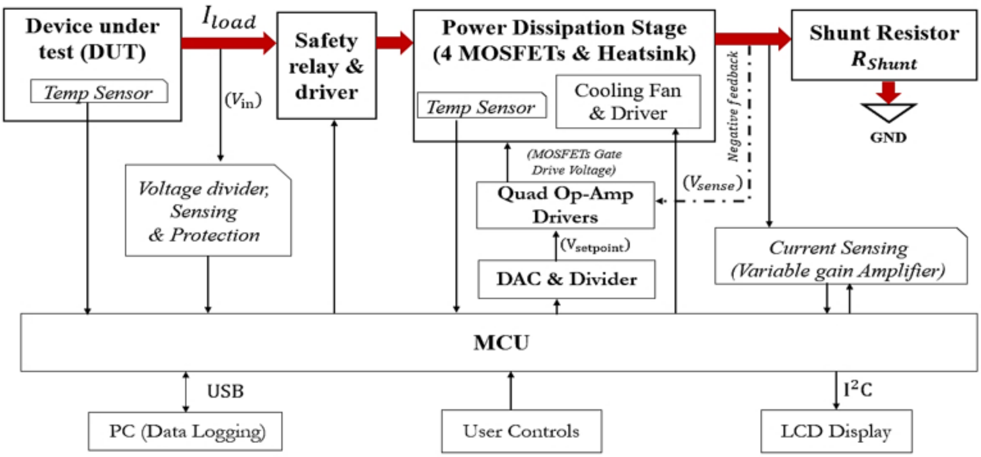

Figure 3: Functional block diagram of the system

2.2.2 Closed-Loop Current Control

The control system consists of a 12-bit digital-to-analogue converter (DAC), a quad operational amplifier, and four parallel power metal-oxide semiconductor field-effect transistors (MOSFETs) for high current operation. The microcontroller drives the DAC to generate a setpoint voltage $V_{setpoint}$. This voltage is scaled by a resistive divider and applied to the non-inverting inputs of all operational amplifiers.

The load current flows through the MOSFETs and a bank of shunt resistors, producing a sense voltage. Each operational amplifier compares this sense voltage with the reference voltage and adjusts the MOSFET gate voltage accordingly. This negative feedback loop maintains the desired current and balances current sharing among the MOSFETs.

2.2.3 Measurement and Protection Subsystems

The voltage of the device under test (DUT) is measured using a resistive divider suitable for the microcontroller's analogue-to-digital converter. The shunt voltage is amplified with a precision operational amplifier. Two selectable gain settings allow accurate current measurement over both low and high current ranges.

Two analogue temperature sensors monitor critical temperatures. One sensor measures the DUT surface temperature for performance analysis, while the second monitors the heatsink temperature for protection. When the heatsink temperature exceeds 65 °C, the microcontroller activates a cooling fan through a bipolar junction transistor (BJT) switch to prevent overheating.

2.2.4 Hardware Implementation

The complete schematic (Figure 4) illustrates the practical realisation of the 300 W programmable DC electronic load using a mixed analogue–digital architecture.

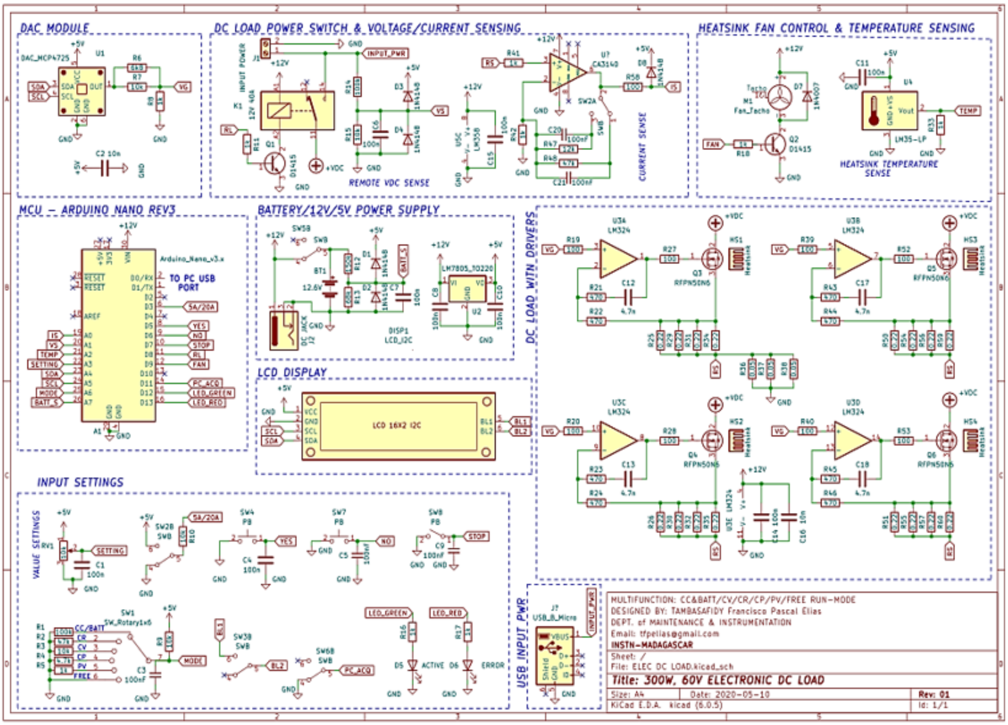

Figure 4: Complete schematic of the 300 W programmable DC electronic load

The system is controlled by an Arduino Nano V3, which communicates with a 12-bit DAC via the I²C interface to generate a precise current reference. This reference voltage is applied to four parallel control loops implemented with an LM324 operational amplifier. Each loop independently drives an RFPN50N6 MOSFET, forming a closed-loop current sink. The feedback is based on the voltage drop across paralleled low-value shunt resistors, allowing regulation of the load current and ensuring current sharing between MOSFETs.

Current measurement is achieved using paralleled shunt resistors combined with selectable gain amplification, enabling accurate sensing over a wide range (0–20 A). The input voltage (up to 60 V) is measured through a resistive divider adapted to the analogue-to-digital converter input range, with remote sensing used to reduce measurement errors due to line resistance.

Thermal monitoring is performed by two LM35 sensors: one attached to the heatsink for protection, and one for measuring the temperature of the DUT. When the heatsink temperature exceeds a defined threshold (65 °C), a transistor-driven fan is activated.

The system is powered from a 12 V source, with linear regulation (LM7805) providing a stable 5 V supply for control circuitry. User interaction is handled through push buttons, LEDs and a 16×2 LCD (I^2C interface), with USB communication for data acquisition.

2.2.5 Physical Implementation

The completed system uses a large heatsink with multiple MOSFETs mounted to ensure effective heat dissipation. A cooling fan is placed above the heatsink. The front panel includes a backlit LCD, rotary encoders for mode selection, a control knob for parameter adjustment, LED status indicators, and input/output terminals. Ventilation openings support airflow and thermal management (Figure 5).

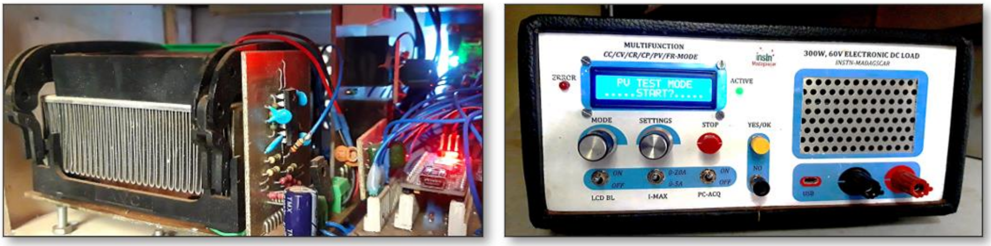

Figure 5: Completed electronic load system: internal construction (left) and user interface panel (right)

2.2.6 Calibration

Accurate calibration is essential to reliable comparative measurements. Voltage and current calibration were performed using a precision reference instrument (Figure 6).

Voltage calibration covered the range from 0 to 55 V. A stable DC power supply provided test voltages in 1 V steps, and readings from the electronic load were compared with those from a Fluke multimeter.

Current calibration was carried out over the 0–20 A range. The multimeter was connected in series with known resistive loads. Separate calibrations were performed for the low-current (0–5 A) and high-current (5–20 A) gain settings to maximise accuracy. Linear regression was applied to determine correction factors implemented in the firmware.

Figure 6: System calibration set-up

2.3 Testing Protocols

2.3.1 PV Module Testing

PV modules were tested under natural sunlight by sweeping the load current from zero to short-circuit conditions (Figure 7). At each step, the voltage and current were recorded to generate complete I–V and P–V curves. To reduce the impact of changing environmental conditions, tests were carried out during clear-sky periods around the solar noon. All comparative measurements were performed in quick succession, and multiple curves were recorded for each module to evaluate repeatability.

Figure 7: PV module test set-ups: 50 W polycrystalline modules (left) and 150 W polycrystalline modules (right)

2.3.2 Battery Capacity Testing

Battery capacity tests were performed using constant-current discharge (Figure 8). The electronic load was set to a fixed current, and discharge was stopped when the cut-off voltage specified by the manufacturer was reached. Voltage, current and time were logged continuously during the test.

Figure 8: Battery test set-ups: 3.7 V/6 800 mAh Li-ion battery (left) and 12 V/10 Ah lead-acid battery (right)

3 Results

3.1 Comparative Analysis of 50 W PV Modules

Two nominally identical 50 W PV modules from different manufacturers were evaluated under stable sunlight conditions. Four I–V curves were recorded for each module and averaged. The results show clear performance differences between the two products (Figure 9).

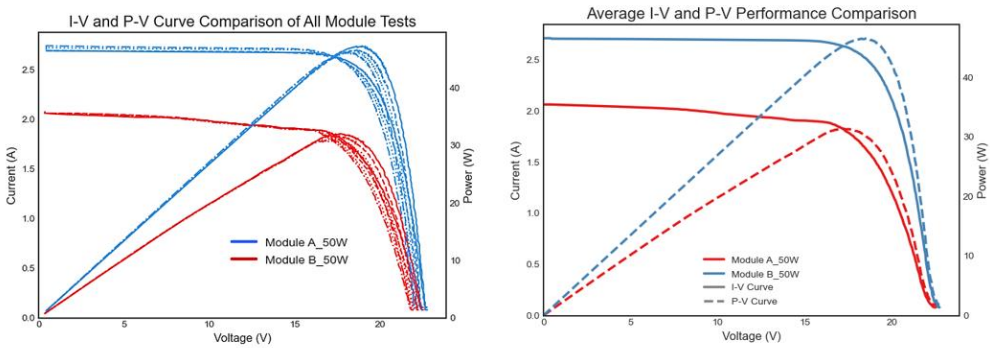

Figure 9: I–V and P–V characteristics of two 50 W PV modules showing performance comparison

Table 1 lists the key electrical performance data.

Table 1: Electrical performance parameters for two 50 W PV modules (mean ± standard deviation, *n* = 4)

Parameter	Module A_50W	Module B_50W
Pmax (W)	31.47 ± 0.51	46.68 ± 0.46
Vmp (V)	17.46 ± 0.24	18.49 ± 0.37
Imp (A)	1.80 ± 0.01	2.52 ± 0.03
Voc (V)	22.10 ± 0.26	22.34 ± 0.25
Isc (A)	2.06 ± 0.00	2.71 ± 0.02
FF	0.690 ± 0.003	0.771 ± 0.005

Module B_50W delivered a maximum power of 46.68 W, corresponding to 93% of its rated value, while module A_50W reached only 31.47 W, or 63%. Both modules showed similar open-circuit voltages near 22 V, but module B_50W exhibited a much higher short-circuit current 2.71 A. Its FF of 0.771 is consistent with good-quality crystalline silicon modules. In contrast, module A_50W had a lower FF of 0.690, indicating higher internal losses. The low spread in repeated measurements confirms that these differences are intrinsic to the modules.

3.2 Comparative Analysis of 150 W Modules

Six 150 W PV modules from three different brands and with different ages were tested under identical conditions. Each module was measured twice to confirm consistency. The modules were grouped as follows:

- Brand X_150W: Module A_150W and Module B_150W, both over 6 years old.
- Brand Y_150W: Module C_150W and Module D_150W, a few months old.
- Brand Z_150W: Module E_150W and Module F_150W, 3 years old.

Figure 10 shows the I–V and P–V curves for all modules, with individual and average brand results. Table 2 summarises the electrical data. The results highlight both inter-brand differences and strong variations between modules of the same brand.

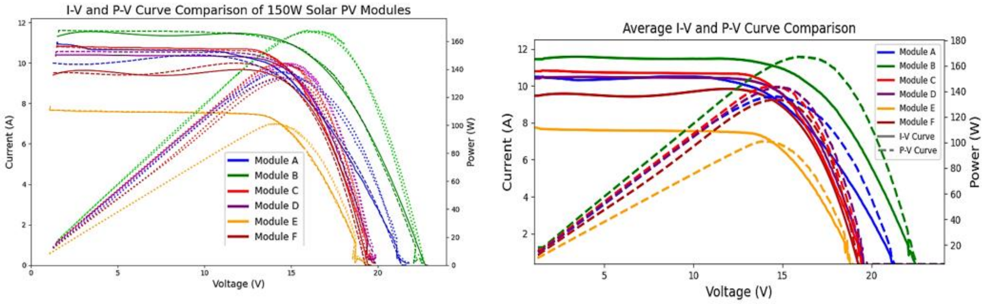

Figure 10: I–V and P–V characteristics for six 150 W PV modules from three manufacturers: individual module curves (left) and averaged curves (right)

Table 2: Measured electrical performance parameters for 150 W PV modules

Module	Pmp (W)	Vmp (V)	Imp (A)	Voc (V)	Isc (A)	ΔP (%)[a]	FF
Module A_150W	135.83	14.68	9.25	21.44	10.48	−9.45	0.604
Module B_150W	167.01	15.93	10.48	22.70	11.43	11.34	0.644
Module C_150W	143.83	14.28	10.07	19.79	10.78	−4.12	0.674
Module D_150W	143.33	15.03	9.54	19.84	10.40	−4.45	0.694
Module E_150W	101.17	14.08	7.19	25.00	7.70	−32.55	0.525
Module F_150W	133.49	14.63	9.13	19.39	9.46	−11.01	0.728

[a] ΔP(%) represents percentage deviation from 150 W nominal rating.

One module from Brand X (module B_150W) exceeded its nominal rating, delivering 167.01 W, while its age-matched counterpart (module A_150W) produced only 135.83 W. Brand Y modules, which were only a few months old, showed very similar performance (143 W) and consistent FFs (~0.68), suggesting stable manufacturing quality. In contrast, one module from Brand Z (module E_150W) exhibited severe degradation, delivering only 101.17 W with a very low FF of 0.525. These results show that performance depends more on manufacturing quality and specific degradation mechanisms than on age alone.

3.3 Battery Discharge Analysis

Battery capacity tests were done on three new lithium-ion batteries and two aged lead-acid batteries. Figure 11 shows their voltage discharge curves, and Tables 3 and 4 presents the performance data.

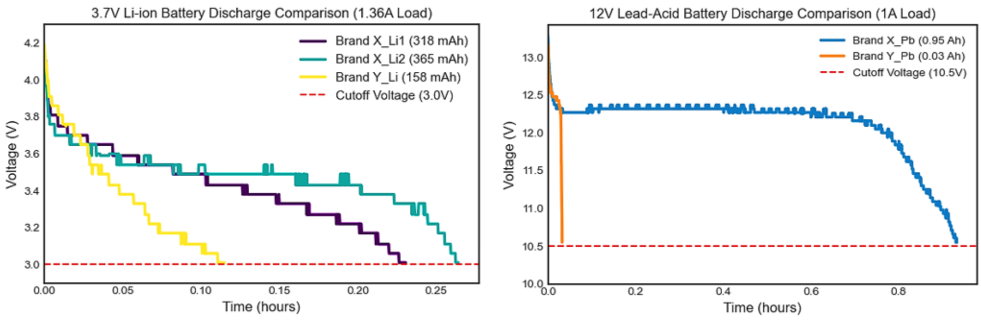

Figure 11: Battery discharge characteristics: three new 3.7 V lithium-ion batteries (left), two aged 12 V lead-acid batteries (right)

Table 3: Measured performance of 3.7 V lithium-ion batteries (advertised capacity: 6 800 mAh)

Battery Name	**Time (min)**	**Avg. Current (A)**	**Avg. Voltage (V)**	**Capacity (mAh)**	**Capacity (%)**	**Energy (Wh)**
Brand *X_Li*1	15.85	1.380	3.48	365	5.37	1.267
Brand *X_Li*2	13.83	1.378	3.43	318	4.68	1.091
Brand *Y_Li*	6.90	1.379	3.39	158	2.32	0.534

Table 4: Measured performance of 12 V lead-acid batteries (nominal capacity: 10 Ah, ~5 years age)

Battery Name	**Time (min)**	**Avg. Current (A)**	**Avg. Voltage (V)**	**Capacity (Ah)**	**Capacity (%)**	**Energy (Wh)**
Brand *X_Pb*	55.93	1.012	12.13	0.948	9.48	11.5
Brand *Y_Pb*	1.95	0.997	12.48	0.032	0.32	0.398

3.3.1 Lithium-Ion Battery

Three new lithium-ion cells rated at 6 800 mAh were tested at a constant discharge current of 1.36 A. All three batteries delivered only a small fraction of their advertised capacity. Measured capacities ranged from 158 mAh to 365 mAh, corresponding to just 2.3–5.4% of the nominal value. The discharge curves confirmed lithium-ion behaviour, but the results clearly indicate severe capacity overstatement and poor-quality control.

3.3.2 Lead-Acid Battery

Two aged 12 V lead-acid batteries were discharged at 1 A to a cut-off voltage of 10.5 V. One battery delivered about 0.95 Ah, or 9.5% of its rated capacity, showing advanced ageing but still limited usability. The second battery failed almost immediately, providing only 0.03 Ah, which indicates complete end of life despite an initially normal voltage.

4 Discussion

4.1 Validation of Low-Cost Characterisation Approach

The results demonstrate that a locally built electronic load can effectively reveal large quality differences in PV modules and batteries. The system identified power differences of up to 33% between identical 50 W modules, wide performance spreads among 150 W modules, and extreme capacity fraud in lithium-ion batteries. Such issues would remain hidden without testing tools. Our system, focused on electrical characterisation, complements other innovative approaches such as automated visual defect detection using artificial intelligence [7]. While our tool assesses overall output performance and electrical losses, image-based methods can precisely identify the nature and location of physical defects (micro-cracks, PID). The future combination of such frugal tools – one for electrical performance and another for physical integrity – could offer a highly comprehensive and field-accessible quality assessment package.

4.2 PV Module Quality Insights

The PV module tests confirm that nameplate ratings are unreliable in unregulated markets. Our findings, showing power deviations up to 33% and variable FFs, resonate strongly with studies using comparable frugal tools, which also report significant performance spreads attributed to manufacturing inconsistencies and degradation [6]. The fill factor proved to be a useful indicator of internal quality and degradation. Modules with low fill factor values showed clear signs of defects or ageing that directly reduce energy yield.

4.3 Battery Quality Insights

Battery testing revealed intentional mislabelling in lithium-ion products and highlighted the limits of age-based assessment for lead-acid batteries. Only direct capacity measurements can reliably determine remaining battery life.

4.4 Limitations

The main limitation of this approach is the use of natural sunlight, which introduces variability due to changing irradiance and temperature. However, this constraint is inherent to portable low-cost testers. Research confirms that the core utility of such tools lies not in absolute precision under STC, but in their ability to provide reliable comparative assessments and detect major faults under identical real-world conditions

[6], which is the primary goal of our system. These effects prevent absolute comparison with STCs, unlike accredited mobile labs which use class A^+ solar simulators and maintain module temperature at 25 °C [5]. However, this variability has limited impact on relative comparisons when products are tested under the same conditions, which is the core objective of this frugal tool for fraud detection and comparative assessment in real-world settings.

4.5 Practical Applications

The proposed system has clear applications in education, procurement, installation and maintenance. It supports hands-on training, helps detect substandard products before purchase, aids field diagnostics, and enables planned battery replacement. The documented battery fraud also highlights the need for regulatory controls in emerging markets.

5 Conclusions

This study confirms the feasibility and practical value of locally developed electronic load systems for PV module and battery quality assessment in resource-limited settings. The 300 W programmable DC load successfully traced I–V and P–V curves under natural sunlight and measured battery discharge capacity. Comparative testing revealed major quality issues, including large power differences between nominally identical PV modules and extreme capacity fraud in lithium-ion batteries. These results demonstrate that significant risks to system reliability and economic viability can be identified using accessible low-cost instrumentation.

Although this approach cannot replace standardised certification procedures, it fills a critical gap between no testing and full laboratory testing. Its strength lies in comparative assessment under identical real-world conditions, fraud detection, maintenance diagnostics, and technical training. For many developing markets, these capabilities are essentials to improve procurement decisions, reduce early system failures, and build local expertise in PV system evaluation.

The work presented here was originally developed in the context of a nanotechnology conference, which highlights an important synergy. Recent advances in quantum dot solar cells, perovskites, and nanostructured materials demand both sophisticated nanoscale characterisation and accessible methods to evaluate the final devices. Our frugal electronic load, although designed for commercial modules, can be readily adapted to test prototypes based on nanomaterials, thereby bridging fundamental research and practical application.

Future improvements may include irradiance sensing, temperature compensation and automated cycling. The evolution of such frugal testers, as seen in related work, points towards integration with the internet of things for remote data logging and the use of algorithms for enhanced diagnostic capabilities [6]. Although research continues to push the limits of PV conversion efficiency towards theoretical maxima above 40% for multi-junction cells and exploring concepts such as intermediate band and hot-carrier solar cells [14], there is a parallel and urgent need for accessible tools that ensure the basic quality and reliability of PV products in emerging markets. This work represents a step towards bridging that gap, proving that meaningful quality assessment can be achieved through frugal innovation and local capacity building.

In addition, the modular architecture of the system makes it suitable for testing emerging nanotechnological devices (for example, quantum dot solar cells) under real-world conditions, therefore contributing to the validation and maturation of next-generation PV technologies.

For battery testing, implementing programmable multistage charge–discharge cycles would enable deeper characterisation, including cycle life estimation, internal resistance evolution, and efficiency analysis. Adding automated cut-off detection and safety interlocks would also protect both the DUT and the operator.

Overall, this work represents a realistic and scalable path towards strengthening solar energy deployment and consumer protection in resource-constrained settings.

6 References

[1] M. de Riso, M. Dhimish, P. Guerriero and S. Daliento, "Design of a Portable Low-Cost I-V Curve Tracer for On-Line and In Situ Inspection of PV Modules," *Micromachines*, vol. 15, no. 7, p. 896, Jul. 2024, doi: 10.3390/mi15070896.

[2] C. Brunet *et al*., "Impacts Generated by a Large-Scale Solar Photovoltaic Power Plant Can Lead to Conflicts between Sustainable Development Goals: A Review of Key Lessons Learned in Madagascar," *Sustainability*, vol. 12, no. 18, p. 7471, Sept. 2020, doi: 10.3390/su12187471.

[3] W. Xiao, *Photovoltaic Power System: Modelling, Design and Control*. Hoboken, NJ, USA: John Wiley & Sons, 2017. https://doi.org/10.1002/9781119280408.

[4] A. Firman, M. Cáceres, A. R. González Mayans and L. H. Vera, "Photovoltaic Qualification and Approval Tests," *Standards*, vol. 2, no. 2, pp. 136–156, Apr. 2022, doi: 10.3390/standards2020011.

[5] J. Coello, L. Pérez, F. Domínguez and M. Navarrete, "On-site Quality Control of Photovoltaic Modules with the PV MOBILE LAB," *Energy Procedia*, vol. 57, pp. 89–98, 2014, doi: 10.1016/j.egypro.2014.10.012.

[6] A. F. Tchouli, S. N. Ngasop, J. H. Tchami, C. B. N. Fapi and H. Tchakounté, "Design and Improvement of an Automated Tool for Quality Control and Performance Assessment of Photovoltaic Modules," *Solar*, vol. 5, no. 2, p. 14, Apr. 2025, doi: 10.3390/solar5020014.

[7] S. Hassan and M. Dhimish, “Enhancing solar photovoltaic modules quality assurance through convolutional neural network-aided automated defect detection,” *Renew. Energy*, vol. 219, p. 119389, Dec. 2023, doi: 10.1016/j.renene.2023.119389.

[8] INSTN-Madagascar. “Contributes to the implementation of nuclear science and technology application projects through the maintenance of scientific equipment.” Accessed: 14 Oct. 2024. [Online.] Available: https://www.instn.mg/?page=site/src/rechercheDev/MI.

[9] R. Baptist, R. Campagnolo and J. P. Rakotoniaina, “Workshop on PV cell Characterizations,” presented at the First Int. NANOMADA Colloq.,” INSTN-Madagascar, 2018.

[10] J. I. Morales-Aragonés, V. A. Gómez, S. Gallardo-Saavedra, A. Redondo-Plaza, D. Fernández-Martínez and L. Hernández-Callejo, “Low-Cost Three-Quadrant Single Solar Cell I-V Tracer,” *Appl. Sci.*, vol. 12, no. 13, p. 6623, Jun. 2022, doi: 10.3390/app12136623.

[11] A. Augusto, A. Killam, S. G. Bowden and H. Wilterdink, “Measuring outdoor I–V characteristics of PV modules and systems,” *Prog. Energy*, vol. 4, no. 4, p. 042006, Oct. 2022, doi: 10.1088/2516-1083/ac851c.

[12] G. Marin-Garcia, G. Vazquez-Guzman, J. M. Sosa, A. R. Lopez, P. R. Martinez-Rodriguez and D. Langarica, “Battery Types and Electrical Models: A Review,” presented at *2020 IEEE Int. Autumn Meet. Power, Electron. Comp. (ROPEC)*, Ixtapa, Mexico, Nov. 2020, pp. 1–6, doi: 10.1109/ROPEC50909.2020.9258711.

[13] Arduino. “Arduino UNO Q: From blink to think.” Accessed: 10 Dec. 2023. [Online.] Available: https://www.arduino.cc/.

[14] J.-F. Guillemoles, “The quest for very high efficiency in Photovoltaic energy conversion,” *Europhys. News*, vol. 41, no. 2, pp. 19–22, Mar. 2010, doi: 10.1051/epn/2010203.